PERGAMON

Journal of Structural Geology 24 (2002) 1463–1478

JOURNAL OF STRUCTURAL GEOLOGY

www.elsevier.com/locate/jstrugeo

The influence of nano-scale second-phase particles on deformation of fine grained calcite mylonites

Marco Herwegh[a,*], Karsten Kunze[b]

[a]*Geologisches Institut, Universität Bern, Baltzerstrasse 1, CH-3012 Bern, Switzerland*
[b]*Geologisches Institut, ETH Zürich, Switzerland*

Received 12 July 2000; revised 1 October 2001; accepted 24 October 2001

Abstract

Grey and white carbonate mylonites were collected along thrust planes of the Helvetic Alps. They are characterised by very small grain sizes and non-random grain shape (SPO) and crystallographic preferred orientation (CPO). Presumably they deformed in the field of grain size sensitive flow by recrystallisation accommodated intracrystalline deformation in combination with granular flow. Both mylonites show a similar mean grain size, but in the grey mylonites the grain size range is larger, the grain shapes are more elongate and the dynamically recrystallised calcite grains are more often twinned. Grey mylonites have an oblique CPO, while the CPO in white mylonites is symmetric with respect to the shear plane. Combustion analysis and TEM investigations revealed that grey mylonites contain a higher amount of highly structured kerogens with particle sizes of a few tens of nanometers, which are finely dispersed at the grain boundaries.

During deformation of the rock, nano-scale particles reduced the migration velocity of grain boundaries by Zener drag resulting in slower recrystallisation rates of the calcite aggregate. In the grey mylonites, more strain increments were accommodated by individual grains before they became refreshed by dynamic recrystallisation than in white mylonites, where grain boundary migration was less hindered and recrystallisation cycles were faster. Consequently, grey mylonites represent 'deformation' microfabrics while white mylonites are characterised by 'recrystallisation' microfabrics. Field geologists must utilise this different deformation behavior when applying the obliquity in CPO and SPO of the respective mylonites as reliable shear sense indicators.

Keywords: Calcite; Mylonite; Organic content; Second phases; Zener drag; Deformation mechanisms; Recrystallisation; Microstructures; Shear sense indicators; Lattice preferred orientation

1. Introduction

When a rock deforms to high strains under constant physical conditions, a steady-state microfabric should develop with a stable bulk grain size distribution, shape preferred orientation (SPO) and crystallographic preferred orientation (CPO). Cycles of nucleation, growth and consumption of individual grains result in a stationary equilibrium of constructive and destructive processes, thus preserving a steady-state microfabric on the bulk average (Means, 1981; Knipe, 1989; Herwegh et al., 1997). The balance between the individual strain accommodating processes and the resulting mechanism assemblage is closely related to the physical conditions of deformation (i.e. temperature, strain rate, fluid properties; see e.g. Schmid et al., 1987; Hirth and Tullis, 1992). From a rheological point of view, de Bresser et al. (2001) suggested that the competition between grain size reduction and grain growth induces a rock strength located at the boundary between the dislocation and diffusion creep fields.

For calcite, different deformation mechanisms are observed in experimentally deformed fine grained aggregates: (a) *Low stress regime (high temperature, slow strain rate)*: diffusion creep accommodated by grain boundary sliding and to a minor extend by intracrystalline deformation (e.g. Schmid, 1976; Walker et al., 1990), (b) *High stress regime (low temperature, fast strain rate)*: recrystallisation accommodated dislocation creep (e.g. Schmid et al., 1987; Rutter et al., 1994; Pieri et al., 2001a,b), (c) *transition regime*: intracrystalline deformation accommodated by grain boundary sliding (Casey et al., 1998).

Natural calcite mylonites that deformed under low-grade metamorphic conditions typically show a fine grain size and often a well-developed CPO (e.g. Schmid, 1981; Schmid et al., 1981; Burkhard, 1990; Busch and Van Der Pluijm, 1995; Bestmann et al., 2000). The CPO observed in calcite mylonites from the Helvetic Alps vary mostly between two types: (a) *symmetric CPO* with a strong *c*-axis maximum

* Corresponding author. Tel.: +41-31-631-8764; fax: +41-31-631-4843.
E-mail address: herwegh@geo.unibe.ch (M. Herwegh).

0191-8141/02/$ - see front matter
PII: S0191-8141(01)00144-4

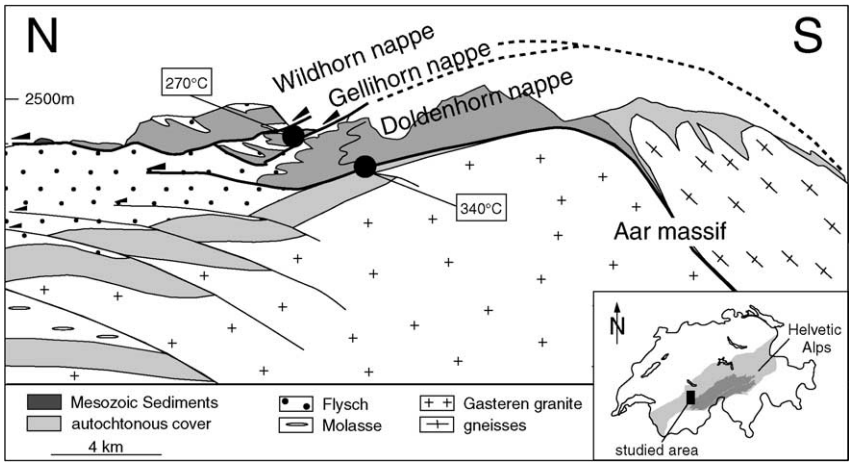

Fig. 1. N–S profile through the studied area in the Helvetic Alps, Switzerland (modified after Pfiffner et al., 1997). Black circles show the two localities investigated.

perpendicular to the foliation and *a*-axes rather randomly distributed within the foliation plane (orthorhombic or axial texture symmetry), and (b) *oblique CPO* with a *c*-axis distribution oblique to the foliation (monoclinic texture symmetry). Using results from numerical modelling of calcite CPO (Wenk et al., 1987), Ratschbacher et al. (1991) interpreted the changes from symmetric to oblique *c*-axis patterns to be a function of increasing amount of simple shear, i.e. of the vorticity (non-coaxiality) in the bulk deformation.

In nature, calcite mylonites are rarely pure monomineralic aggregates. They often contain variable amounts of second phases (e.g. mica, dolomite, quartz, organic matter, ore minerals), which certainly influenced the way to a steady state in microstructure and mechanical behaviour and also the optical appearance (the latter discussed by Schmid, 1997). It is well known from metal physics that fine dispersed second phase particles cause a retarding force on migrating subgrain and grain boundaries in the matrix (called Zener drag), thus hindering recovery and recrystallisation (Hornbogen and Köster, 1978; Olgaard and Evans, 1986; Humphreys and Hatherly, 1996, Chapter 8). In such materials, more aspects of a deformation microstructure and stronger deformation texture components remain compared with pure aggregates, which may obtain a recrystallisation texture and microstructure under equivalent conditions (Doherty et al., 1997). The retarding force increases with increasing volume fraction of the particles and with decreasing particle size, thus strongly with increasing number of particles, and depends sensitively on their spatial dispersion. Under certain conditions, the pinning pressure may be too small to account for a retardation of recrystallisation growth, but sufficient for particle-inhibition of nucleation. On the other hand, larger particles (above 1 μm) cause deformation heterogeneity in the surrounding matrix, thus increasing the stored energy. They may actually act as nucleation sites at which recrystallisation originates (particle stimulated nucleation). While the latter effect tends to promote recrystallisation, the first one is hindering recrystallisation. The competition between both effects depends strongly on number, size, shape and spatial distribution of the particles.

The influence of second-phase particles on the rheology of rocks was investigated by several authors (e.g. Urai et al., 1986; Drury and Urai, 1990; Olgaard, 1990). Minor amounts of second-phase particles can make the rock either (a) weaker or (b) harder than a pure aggregate. (a) The calcite grain size can be maintained to be small (smaller than the equilibrium recrystallised grain size) if pinning by second-phase particles prevents grain growth. In the grain size sensitive field, the smaller grain size corresponds to a lower rock strength (Olgaard, 1990). (b) If grain boundaries drag second-phase particles, i.e. they move with reduced velocity, then the recrystallisation rate is reduced. Higher defect densities cause the impure rock to be harder than the pure aggregate, while the average grain size may be similar for both (Walker et al., 1990).

In this paper we describe the differences in microfabrics and composition between grey and white calcite mylonites and address the following questions. What causes the difference in optical appearance? What is the influence of second-phase particles? What consequences can be inferred on the deformational behavior of these mylonites and what are the geological implications?

2. Regional geological setting and field observations

Carbonate mylonites were collected from two basal thrust planes of the Helvetic nappes in central Switzerland, the Gellihorn and Doldenhorn nappes (Fig. 1). Both nappes were thrust towards NW during Oligocene to Miocene in the Prabé and Kiental phases. The estimated displacements for the Doldenhorn and the Gellihorn nappes are about 5–10 and 8 km, respectively, which were accumulated in shear zones of a few metres thickness (Burkhard, 1988). Fluid inclusion data from quartz veins indicated peak

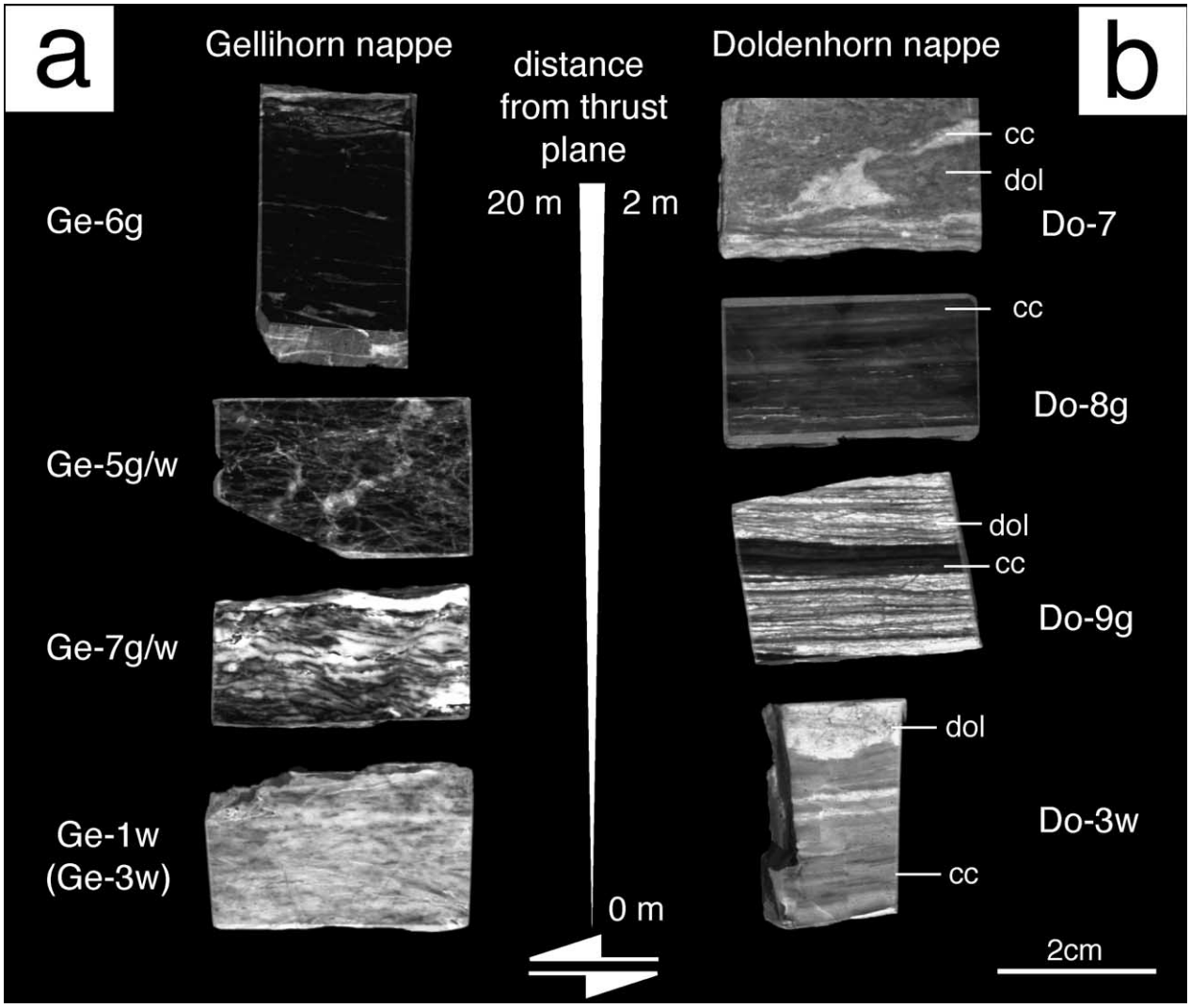

Fig. 2. Sequence of polished rock chips sampled perpendicular to the thrust planes of (a) Gellihorn nappe and (b) Doldenhorn nappe (cc: calcite, dol: dolomite). Reference orientation chosen parallel to the shear zone boundaries if available, otherwise to the foliation.

metamorphic temperatures of 270 °C for the studied location in the Gellihorn nappe (Frey et al., 1980). Calcite–dolomite thermometry gave a peak temperature of 340 °C for the outcrop sampled at the base of the Doldenhorn nappe (Burkhard, 1990).

Along the basal thrust of the Gellihorn nappe limestone (limestone of Quinten) boudins with dimensions of several hundred metres are aligned. At the locality investigated (Swiss coordinate system 625′250/151′200) the limestone has a thickness of about 20 m. The carbonate shows a transition from a dark grey to a white colour with increasing proximity to the thrust contact, which is basically due to an increasing number of white calcite veins (Fig. 2a). In the middle part of the profile the veins show various orientations, while towards the thrust plane they appear more deformed and become more and more parallel to the main foliation.

The base of the Doldenhorn nappe (622′700/144′525) is built up by a carbonate series 2–3 m thick, which can be followed over several kilometres. The sequence consists of white calcite, grey calcite and yellowish dolomitic layers (Fig. 2b). The dolomitic layers are broken, boudinaged and dissected by calcite veins. Both the white and grey calcitic parts form homogeneous and continuous layers in the range of millimetres to few centimetres thickness. In the grey mylonites, patches of dark grey occur, which are surrounded by areas of a brighter grey with diffuse contacts (like Do-8g in Fig. 2b).

No reliable strain markers were found to estimate finite strains for the different constituents inside the zones, apart from the macroscopic bulk estimation from above. The shear zone geometry of the mylonites in the Gellihorn nappe shows anastomosing white bands surrounding grey cores. A layer parallel geometry of both mylonite types dominates in the Doldenhorn nappe.

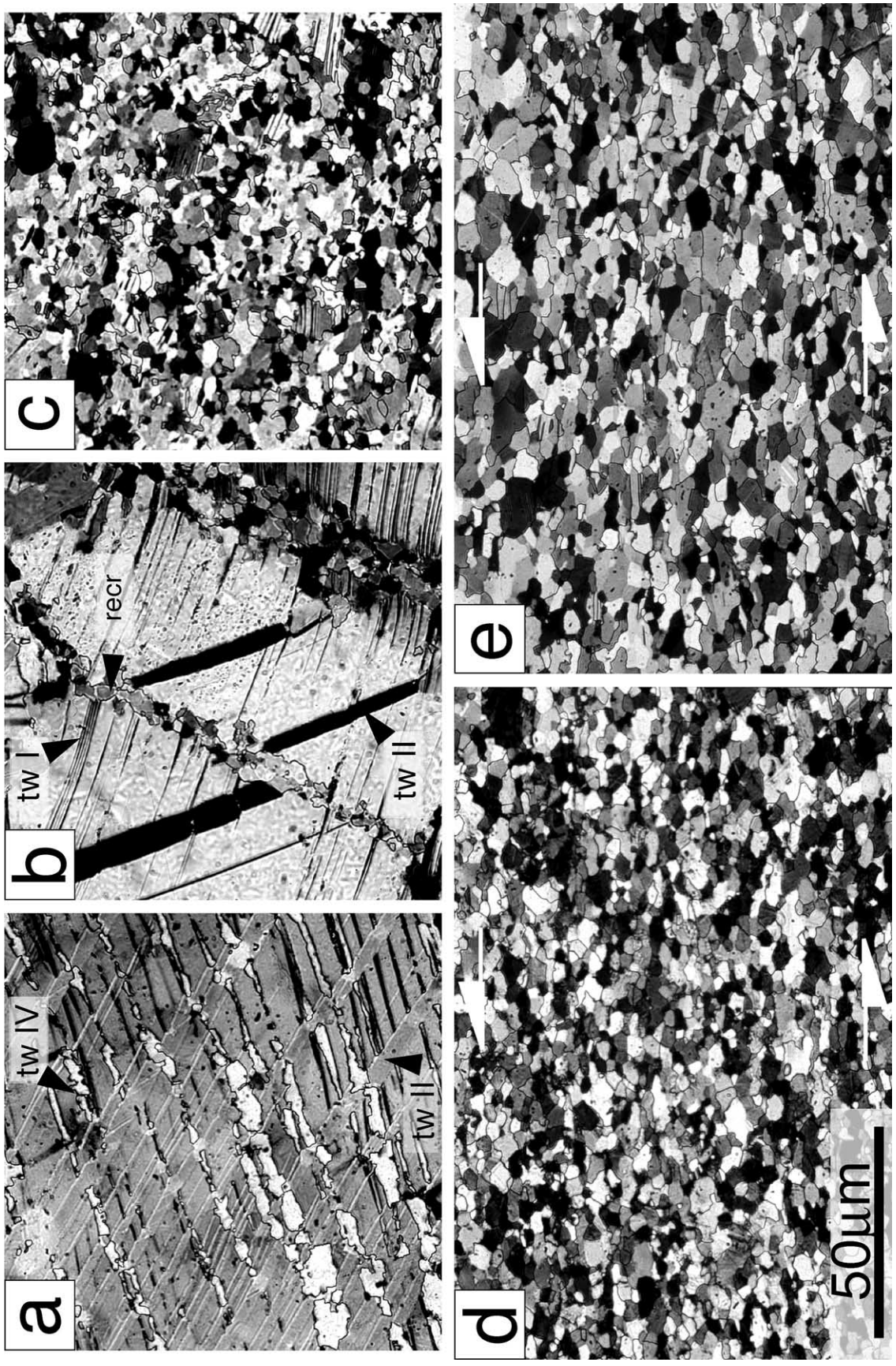

Fig. 3. Optical photomicrographs (crossed polarisers) of ultra-thin sections. (a)–(c) White vein calcite of the Gellihorn nappe with increasing amount of recrystallisation from (a) to (c), (d) white and (e) grey calcite mylonites from the Doldenhorn nappe (tw: twin types after Burkhard (1993); recr: recrystallised grains). Scale bar and shear sense indicator apply to all.

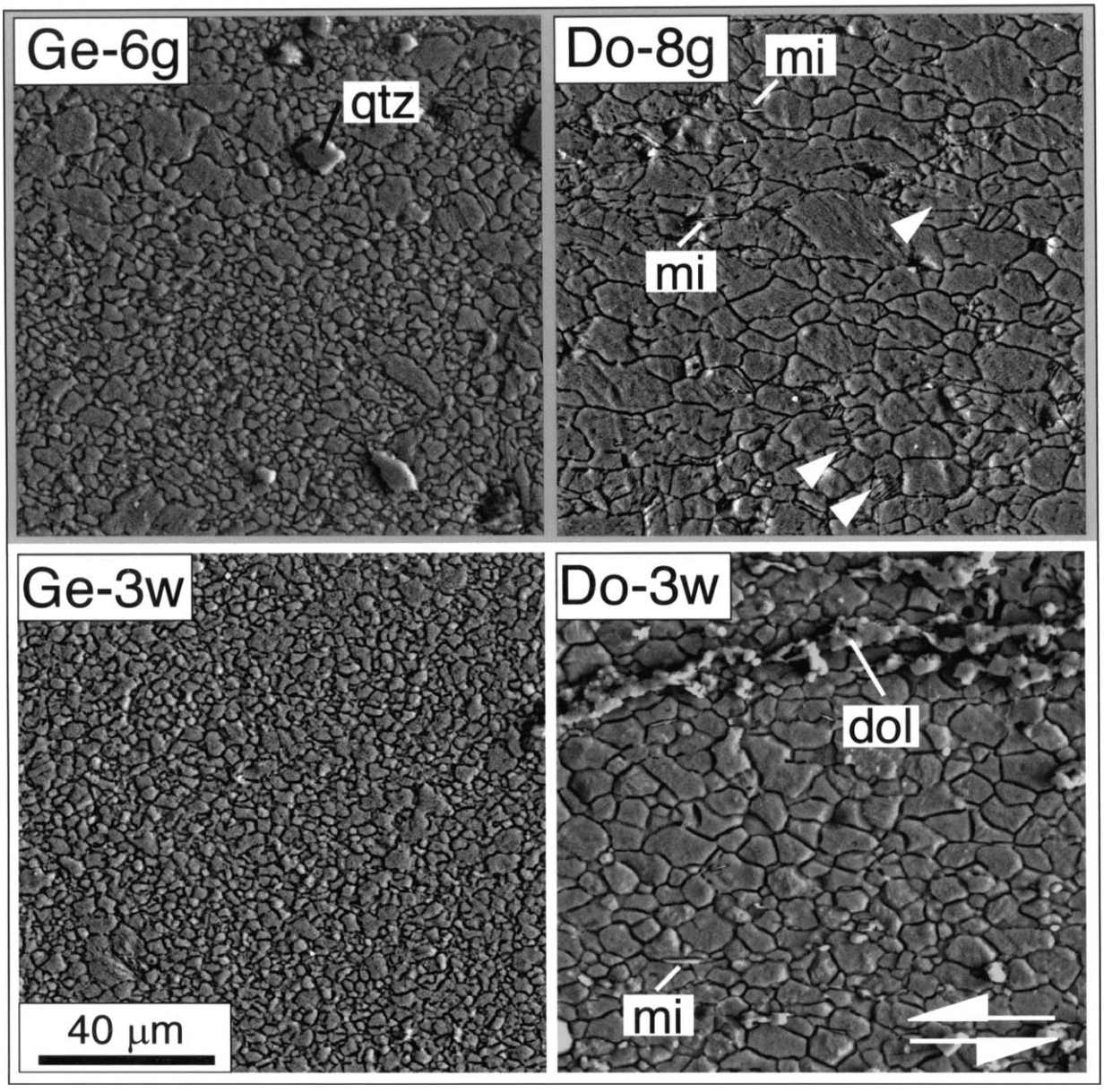

Fig. 4. BSE micrographs of etched bulk surfaces of grey (top) and white (bottom) calcite mylonites from the Gellihorn and Doldenhorn nappes (qtz: quartz, dol: dolomite, mi: mica). Scale bar and shear sense indicator apply to all. Arrows indicate twinned grains.

3. Sample preparation and analytical methods

For both localities investigated, a sample of grey and white mylonites were studied in detail. Ordinary thin sections, ultrathin sections and polished bulk samples were prepared from chips of oriented handspecimens cut parallel to the stretching lineation and perpendicular to the inferred kinematic shear plane. The latter was defined either by the shear zone boundary or the mesoscopic foliation, which are both assumed to be parallel to each other at very high shear strains. The surface of polished bulk chips was etched by a multistage etching technique applying weak acids to visualise the calcite grain boundaries (for details see Herwegh, 2000). Backscatter electron (BSE) images of the etched surfaces were captured digitally using a scanning electron microscope (SEM) CamScan CS4 with a Noran Voyager 4 acquisition system. They were used for grain size and SPO analyses (PAROR: Panozzo, 1983) of the calcite aggregates. For estimation of the calcite grain sizes both the number and area weighted size histograms (i.e. number and area fractions) were calculated.

CPOs were measured in completely and homogeneously recrystallised parts of ultrapolished bulk samples using electron backscatter diffraction (EBSD) for technical details see Pieri et al., 2001a). For each sample, an automated acquisition scan was carried out collecting between 2600 and 18,000 orientation measurements. The step sizes of the measurement grids were chosen to exceed the average

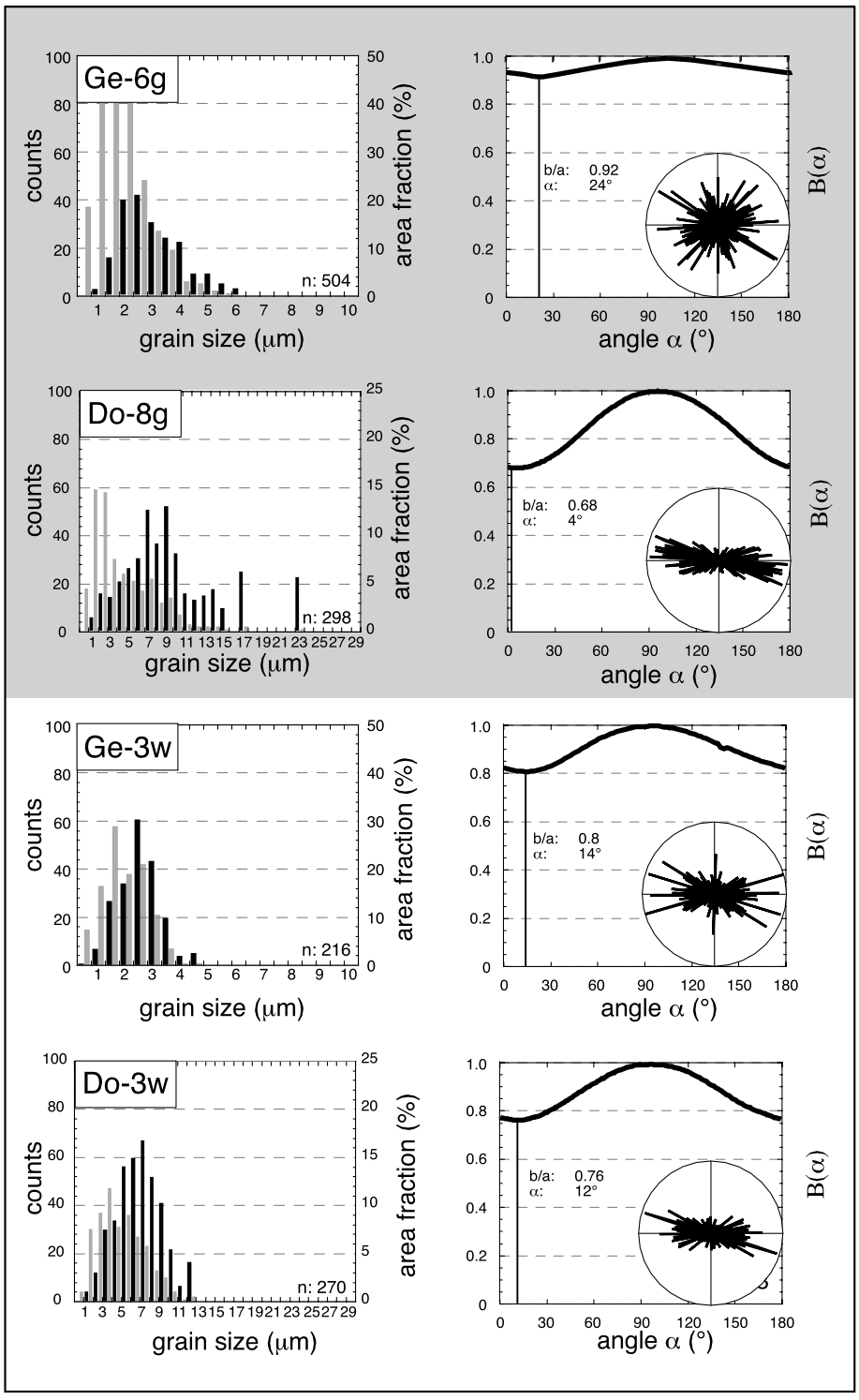

Fig. 5. Two-dimensional grain size and grain shape analyses of grey and white mylonites. Left column: grain size histograms show number of grains (grey bars) and area fractions (black bars) per grain size interval. Right column: grain shape distributions presented by projected average grain dimension $B(\alpha)$ as a function of the projection angle α (for details see Panozzo, 1983). The orientation frequency of the grain long axes are additionally given in rose diagrams.

grain size in the samples, so that adjacent sampling points mostly do not belong to the same grain.

In order to gain information about the size and distribution of second-phase particles, we applied a number of approaches. (a) Insoluble second phases with at least micrometre-dimensions like dolomite, quartz, mica, apatite and hematite can easily be recognised on etched sample surfaces in the BSE images. For these particles, element distribution maps were generated to quantify the modal compositions. (b) The occurrence and distribution of second-phase

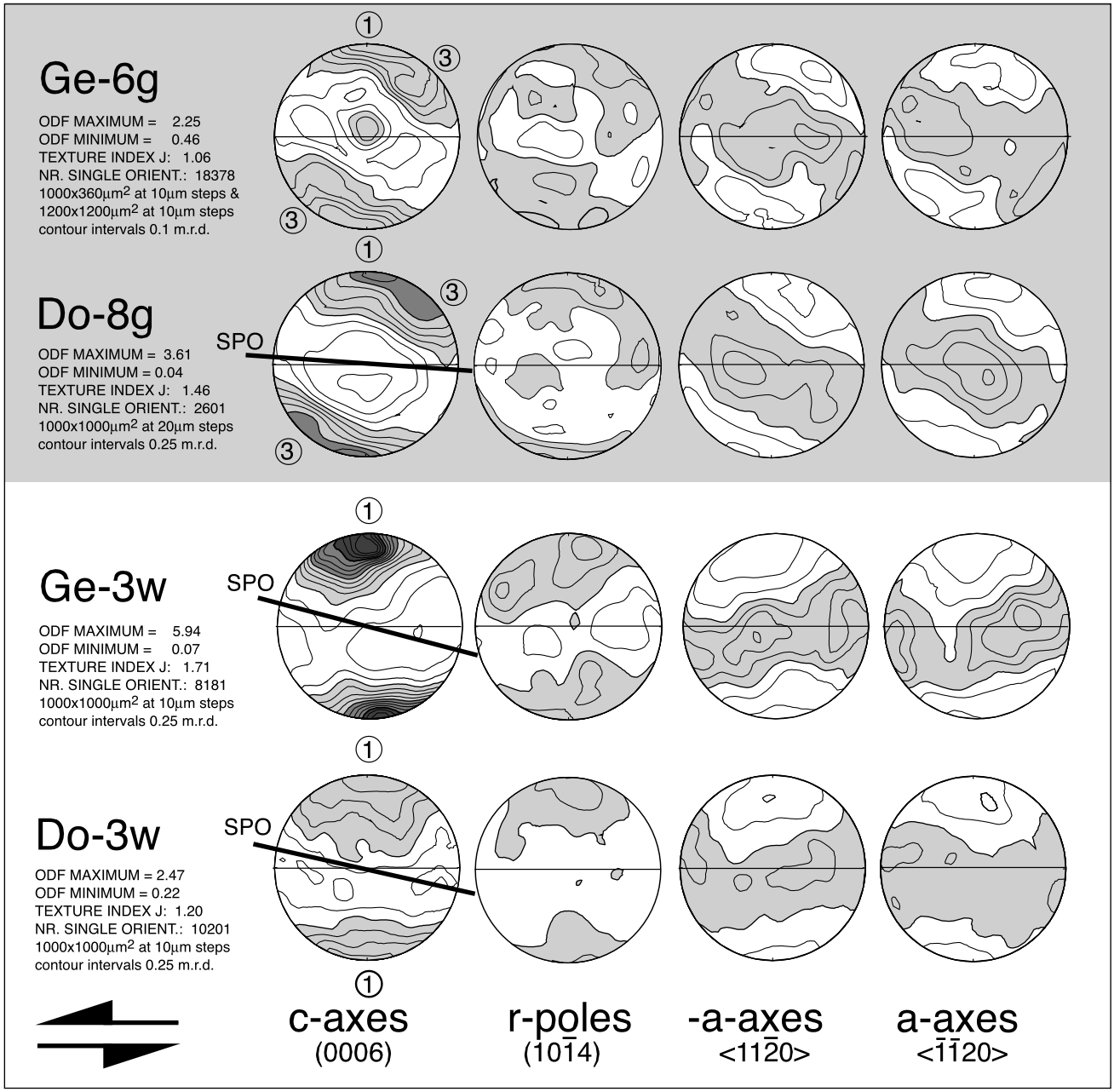

Fig. 6. CPO of grey and white mylonites presented as pole figures. ODF parameters, number of data and dimensions of EBSD measurement grids are indicated. Pole densities above 1.0 m.r.d. (multiples of random distribution) shaded. Traces of the average grain elongation (SPO) are indicated. Numbers in circles refer to *c*-axis maxima according to Schmid et al. (1987).

particles was studied on surfaces of fractured calcite aggregates by high resolution secondary electron (SE) imaging using a SEM (Jeol JSM-6300F) with field emission gun. (c) Second-phase particles with nano-scale dimensions were analysed by decarbonising the milled sample for 24 h in 10% hydrochloric acid and afterwards hot hydrochloric acid for 1 h. The insoluble residue was then weighted and studied on a Hitachi 600 transmission electron microscope (TEM). (d) Type and content of organic matter in the decarbonised residue of the rock powder were analysed using a Leco RC-412 combustion analyser (Cizek et al., 1990). (e) Thin sections of the mylonites, polished on both sides, were ion etched and prepared for TEM investigations to locate the sites of small scale second-phase particles in the microfabric.

4. Microscopic and chemical sample characterisation

4.1. Microstructures

The microstructures of the grey and white Gellihorn

Table 1
Mineral modal compositions of the samples investigated. Feldspars, quartz, apatite and ore minerals occur as accessories with <0.1 vol%. Data are given in vol% based on point counting

Sample	Calcite	Dolomite	Mica
Ge-6g	100.0	–	–
Do-8g	98.7	1.1	–
Ge-3w	100.0	–	–
Do-3w	96.0	1.5	2.8

mylonites are both characterised by a very small grain size of a few micrometres (Figs. 3 and 4). In the white mylonites, calcite veins with a variable degree of dynamic recrystallisation are present, allowing a relative age dating of the different veins. Calcite grains of younger veins are coarser grained and intensely twinned. The youngest twins are thin and straight (type I), while the older ones are thicker, dissected and show twin boundary migration (type II and IV; types after Burkhard, 1993). The occurrence of twin boundary migration (Fig. 3a) indicates a temperature higher than 250 °C (Burkhard, 1993). This is in agreement with the temperatures derived from fluid inclusion data mentioned above. With increasing shear strain (i.e. age), dynamic recrystallisation reduced the grain size (Fig. 3b) producing a very fine-grained recrystallised matrix with only a few twinned remnants of the original vein calcite (Fig. 3c). Thus a sequence of brittle deformation, calcite dissolution–precipitation, followed by intracrystalline deformation and dynamic recrystallisation can be inferred to be responsible for the formation of the white mylonites. The grey mylonite shows a fine grain size as well, but as it originated from a micritic protolith, the grain size must have clearly increased during deformation and recrystallisation. The occurrence of stylolites in the grey mylonites indicates calcite dissolution with precipitation into opening veins.

The white and grey mylonites of the Doldenhorn outcrop (Figs. 3 and 4) are not dissected by calcite veins. Here, the places indicating cycles of brittle deformation and calcite dissolution–precipitation are restricted to the dolomitic layers (Herwegh, 2000). The grain boundaries of the recrystallised calcite grains are mostly straight for both types. A few recrystallised grains in the grey mylonites show twinning, and twinning is even less pronounced in the white calcite aggregates.

4.2. Grain size and shape preferred orientation

The grain size of the recrystallised grains (average weighted by area fractions) is clearly larger in the Doldenhorn (7–8 μm) than in the Gellihorn (2–3 μm) nappe (Figs. 3–5). Within each nappe, the average grain sizes of white and grey mylonites are identical. However, the grain size distributions (area fractions) differ between both types. They show a symmetric Gaussian shape with a smaller grain size range (Gellihorn 0–4.5 μm, Doldenhorn 0–12 μm) for the white mylonites, while those of the grey mylonites reflect an asymmetric distribution with a tail towards larger grain sizes in a wider grain size range (Gellihorn 0–6 μm, Doldenhorn 0–23 μm).

The grain shapes (Fig. 5) of recrystallised calcite grains are more elongated in the Doldenhorn (*b*/*a*: 0.68–0.76) than in the Gellihorn (*b*/*a*: 0.8–0.92) nappe. The average orientation of the grain long axes is slightly oblique with respect to the reference shear plane in the white mylonites (12–14°) but nearly parallel to the reference for the grey mylonites (3–4°).

4.3. Crystallographic preferred orientation

The CPO (or 'texture') show clearly developed patterns with weak to moderate intensities (Fig. 6). In the grey mylonites, two *c*-axes maxima exist: one dominant maximum (marked as 1) normal to the reference plane and the second maximum (marked as 3) 40° disposed towards the lineation opposite to the sense of shear. The *a*-axes are distributed along great circles oblique to the reference plane. This orientation distribution, which is oblique with respect to the reference plane opposite to the inferred shear sense (*monoclinic symmetry*), is similar to other examples from naturally (Ratschbacher et al., 1991) and experimentally deformed calcite aggregates (e.g. Schmid et al., 1987; Casey et al., 1998; Pieri et al., 2001a) and agrees with texture simulations (Wenk et al., 1987).

In the white mylonites, *c*-axes are clustered in a single maximum almost normal to the reference plane and *a*-axes are spread along great circles nearly parallel to the reference plane. Minor maxima of *a*-axes within these girdles exist, but do not correspond to a single crystal orientation as clearly as shown by Bestmann et al. (2000). Thus, the texture in the white mylonites is rather symmetric (*orthorhombic or axial symmetry*) with respect to the reference frame.

Table 2
Content of insoluble residue, organic C and S. Data for insoluble residue are given as total wt%, for organic C and S as wt% of the insoluble residue

Sample	Insoluble residue	Org. C peak A in insoluble residue	Org. C peak B in insoluble residue	S in insoluble residue
Ge-6g	0.69	0.98	9.06	1.5
Do-8g	1.07	0.82	1.02	0.2
Ge-1w	1.29	1.67	0.27	0.1
Do-3w	1.89	0.95	0.06	0.1

4.4. Second-phase particles

All samples studied are very poor in second-phase minerals with sizes above a micron. Image analysis on selected areas revealed a maximum content of microscopic second phases in the range of 1–4 vol% (Table 1). The samples contain insoluble residues between 0.7 and 1.9 wt% (Table 2).

A large amount of extremely fine grained nano-scale particles appeared in the insoluble residues of grey mylonites on TEM images, while similar particles are very rare in the white mylonites (compare Fig. 7a and b). The clustering of particles in Fig. 7a is presumably due to TEM sample preparation. The particles are equiaxed platelets and their dimensions lie in the range of 10–50 nm (Fig. 7c). Flakes of similar shape and dimensions are found within the original aggregates from the grey mylonites, observed in ion-etched TEM samples (Fig. 7d) and on fractured sample surfaces (Fig. 7e), where they are mostly dispersed along grain boundaries and accumulated at triple junctions. These flakes are distinguishable from a few dark squares and rhombs located on some calcite grain boundaries, which are interpreted to present ore minerals and dolomite, respectively. Both TEM (not shown) and SEM (Fig. 7f) images of white mylonite do not show such nano-scale particles, but smooth and straight grain boundaries of calcite.

Combustion analysis revealed differences in type and amount of organic matter between white and grey mylonites, although the bulk organic content does not allow a strict discrimination (Table 2). Two CO_2 peaks are present (Fig. 8): peak A at about 300 °C and peak B at about 550 °C. Both CO_2 peaks are associated with a rise in H_2O and therefore attributed to kerogens. As CO_2 and H_2O combustion relates increasing temperature to an increase in the structural order of the kerogen, we consider peaks A and B as indicators for weakly and highly ordered kerogens, respectively. The important feature is that peak B predominates in the grey samples while in the white ones only peak A exists. In a more quantitative manner this means that the amount of highly ordered organic matter is up to one order of magnitude higher in the grey limestones than in the white ones (Table 2). We identify the above described nano-scale platelets observed by electron microscopy with these highly ordered kerogens, since both features are unique to the grey mylonites. Finally, the sulphur content in grey mylonites is slightly higher than in white mylonites (Table 2), also indicating a higher content of organic matter in the grey ones.

5. Discussion

5.1. Second-phase content

A variety of second phases in the size range from tens of nanometres to micrometres was observed in the investigated mylonites based on a combination of data sets obtained with different analytical methods. In this paragraph, we attempt a synthesis and interpretation of the various observations.

The insoluble residue contained basically all non-carbonate constituents at all scales in the bulk sample. A few large micrometre-scale mineral grains with higher density (e.g. ore minerals, quartz, sheet silicates) cover a major fraction of the residue weight, while low-density nano-scale particles (e.g. organic carbon) do not much contribute to the total. As all samples contained a certain (somewhat heterogeneously distributed) amount of mineralic second-phases of micrometre-scale sizes, the total weight fractions of the insoluble residue did not indicate any clear differences between grey and white mylonites. Since the absolute percentage of mineralic second-phases is very small, they have nearly no influence on the calcite microstructure, and in particular cannot account for the differences between grey and white mylonites. In addition, the grain size, SPO and CPO analyses were performed on carefully selected sample areas with a minimum content of micrometre-scale particles.

Compared with bulk techniques for extracting and analysing the insoluble residue, the image based methods are more specific but limited in their statistical significance, because they typically cover small two-dimensional section cuts of the microstructures. After extended screenings we feel confident to summarise our observations as follows. (a) The number of micrometre-scale second-phase minerals is significantly too low to considerably influence the calcite microstructure. (b) Electron microscopy of the insoluble residue and on fractured surfaces shows an abundance of nano-scale particles mostly along grain boundaries in the grey mylonites, which are not observed in the white mylonites. (c) Highly structured kerogens preferentially occur in grey mylonites, while less structured kerogens exist in similar amounts in both mylonite types. (d) We identify the nano-scale flakes imaged by electron microscopy primarily with the highly structured kerogens detected by combustion analysis. (e) Few additional nano-scale particles like ore minerals and dolomite are observed in the calcite aggregates of grey mylonites. Though we did not attempt a unique identification, those mineralic phases are clearly discriminated from the organic matter by particle shapes.

In summary, both mylonites are comparably pure calcite rocks, but the grey mylonites contain a considerably higher amount of nano-scale organic matter identified as highly structured kerogens.

5.2. Influence and origin of organic carbon

The optical appearance of limestone may depend on various physico-chemical parameters like calcite grain size, small scale second-phase minerals (e.g. pyrite or quartz) and content of organic matter (see Schmid, 1997 and references therein). As there is little difference between

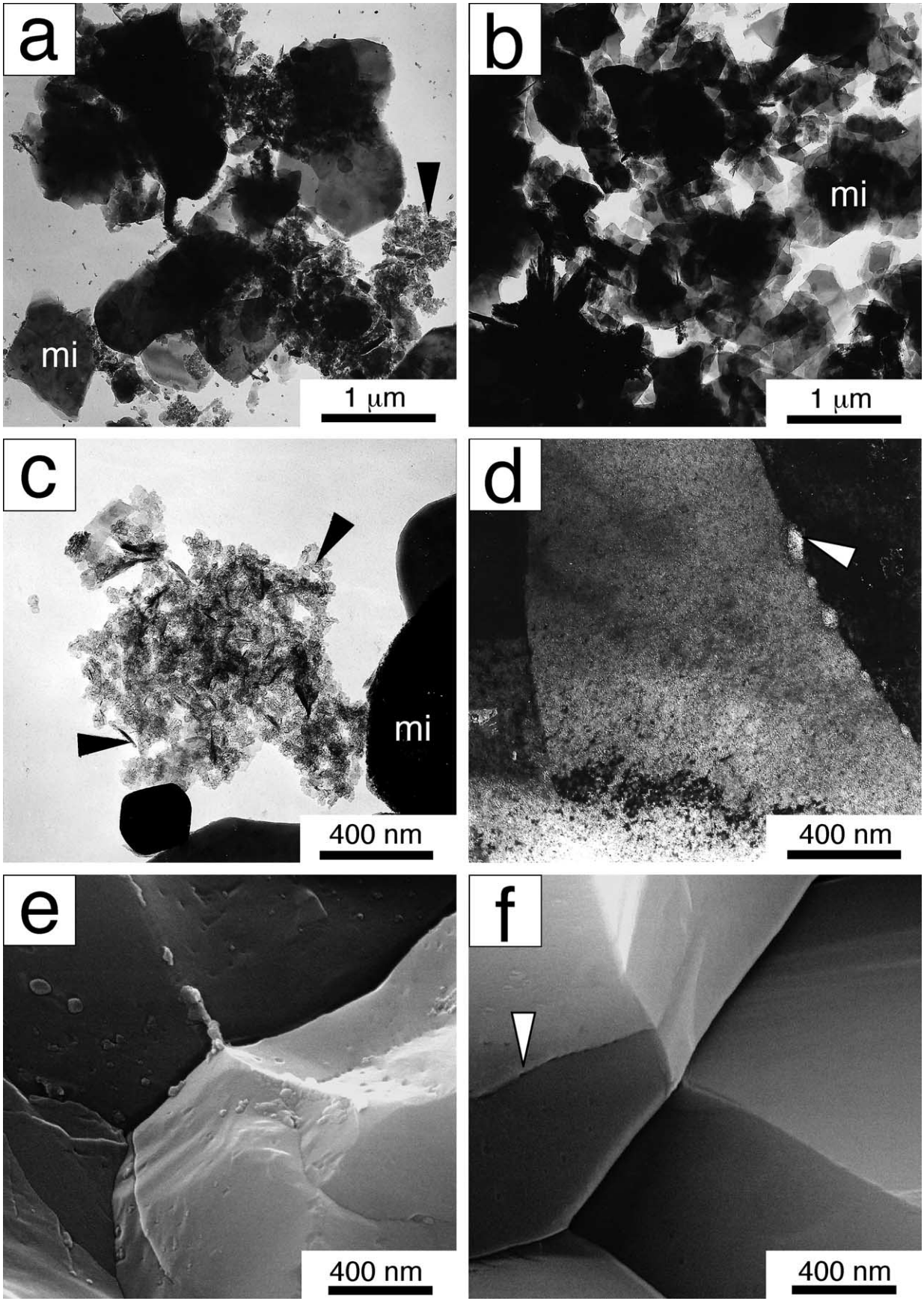
a
mi
1 μm
b
mi
1 μm
c
mi
400 nm
d
400 nm
e
400 nm
f
400 nm

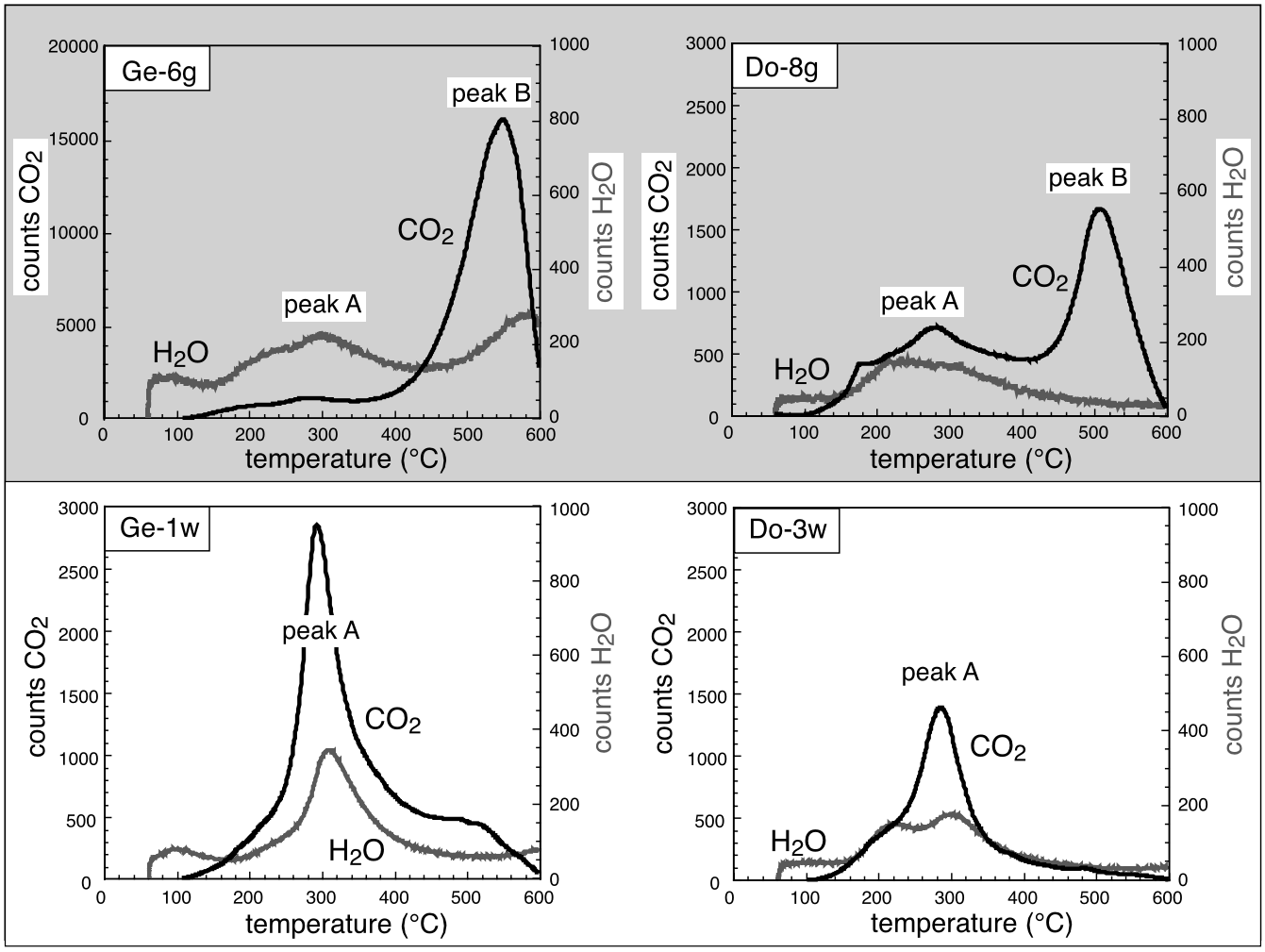

Fig. 8. Combustion analyses of grey (top) and white (bottom) mylonites. Diagrams show the CO_2 and H_2O produced (in relative units) with increasing temperature. Note the predominance of peak B in grey mylonites and of peak A in white mylonites.

the grey and white mylonites within either nappe with respect to the average grain size and to the content of micrometre-scale second-phase minerals, the larger content of nano-scale highly structured kerogen particles in grey mylonites is inferred to be responsible for the grey tone. These kerogens may ultimately transform into graphite at higher temperature, similar to the fine coating on calcite grains reported by Van Der Pluijm (1991) for ultramylonites that deformed at 475 ± 50 °C.

The different kerogen concentrations may be caused by a variety of reasons. (a) Sedimentation of calcite micrites was accompanied by a variable input of organic matter. This could also explain the carbonate sequence observed in the Doldenhorn nappe. (b) Cycles of brittle deformation, calcite dissolution/precipitation and plastic deformation with some fluid flow transformed a grey limestone into a white one, as described above for the Gellihorn mylonites. Nano-scale kerogens of higher structural order remained as insoluble residue within stylolites and along grain boundaries of the grey host rock, while dissolved calcite was transported away by fluids and precipitated in newly generated calcite veins. (c) Bulk dissipation of organic matter resulted in a brightening of the rock appearance. Schmid (1997) showed that, for carbonate rocks affected by contact metamorphism of the Adamello pluton, this process is a function of increasing temperature, where the transition from grey to white mylonites occurs in a temperature range between 450 and 500 °C under static conditions. The bleached regions in the grey

Fig. 7. Electron microscopy of nano-scale particles in grey (sample Ge-6g) and white mylonite (Ge-3w). (a) TEM photograph of the insoluble residue (Ge-6g) shows mineral content (mi: mica) and organic matter in the form of nano-scale particles (arrow). (b) TEM photograph of the insoluble residue (Ge-3w) shows only micas and no nano-scale flakes. (c) TEM photograph shows platy shapes of nano-scale particles (arrows, Ge-6g). (d) TEM photograph of ion-etched calcite aggregate (Ge-6g). Nano-scale particles are mostly located at calcite grain boundaries. (e) SE image of fractured bulk surface (Ge-6g) with nano-scale particles dispersed on the fractured surfaces (grain boundaries) and accumulated along triple junctions. (f) SE image of fractured bulk surface (Ge-3w) with smooth grain surfaces and no nano-scale particles. Some pores are aligned along triple junctions (arrow).

mylonite Do-8g (Fig. 2) indicate that this process could have been activated in deforming rocks even under lower greenschist facies metamorphic conditions.

5.3. Rates of dynamic recrystallisation and microfabric resetting

Based on the large-scale geological settings, the shear strain accommodated by the mylonites along the thrusts should be high enough to establish steady state microfabrics. The existence of SPO and CPO gives indications for intracrystalline deformation by slip and twinning. As the grey and white mylonites should have deformed under identical physical conditions, the differences in their textures and microfabrics must be related to the only difference, which is the different content of nano-scale particles.

Fine dispersed particles affect migrating grain boundaries in two ways. Grain boundaries can either be pinned, i.e. they become immobile, or they can be dragged, which reduces the migration velocity of the grain boundaries (e.g. Urai et al., 1986; Olgaard and Evans, 1988; Evans et al., 2001). Based on the microscopic observations in the grey mylonites, dragging of grain boundaries is more likely to have occurred than pinning. The driving forces of grain boundary migration, which are gradients in strain and surface energy, have to exceed the counteracting dragging force induced by the second-phase particles, causing a retardation of grain boundary migration recrystallisation. In a slower life cycle of nucleation, growth and consumption each individual grain has to accommodate more deformation by intracrystalline glide and to some extent twinning. This results in an asymmetric size distribution of calcite grains (towards larger grain sizes), in more elongate grain shapes and therefore in a more pronounced SPO of the calcite aggregate oriented closely to the foliation plane. Slip and twinning lead to the deformation texture with oblique maxima relative to the shear plane.

In the white mylonites, less kerogen particles means less dragging. The recrystallisation cycles are therefore shorter, so that each individual grain accommodated less strain before it was consumed again. This caused a symmetric, Gaussian shaped grain size distribution, modest grain shape elongation and the SPO more steeply inclined relative to the shear plane. The CPO is dominated by orientations of the recrystallisation texture, which have the *c*-axis normal (thus symmetric) to the shear plane.

5.4. Deformation and recrystallisation textures

In the previous paragraph, oblique and symmetric CPO in grey and white mylonites were referred to as deformation and recrystallisation textures, respectively. Alternative explanations for the differences in texture symmetry shall be discussed in the following. It is generally accepted (e.g. Kocks et al., 1999) that deformation by slip and twinning causes preferred orientations of crystals, which evolve at fixed positions with respect to the kinematic reference frame. With increasing strain, the texture strength usually increases without changing the overall texture pattern. Transitions in the CPO patterns do not simply happen with strain, but arise from changes in the active slip systems (usually related to gradients in temperature), in the deformation path (principal strains and vorticities) or in the dominant deformation processes (e.g. with or without recrystallisation). The first possibility is excluded in our case, as no temperature gradients could have existed between grey and white mylonites over distances of a few metres.

5.4.1. Different finite shear strains

Texture transitions with progressive finite strain (under constant deformation conditions and kinematics) were observed in high strain shear experiments of Solnhofen limestone (Schmid et al., 1987; Casey et al., 1998), Carrara marble (Schmid et al., 1987; Pieri et al., 2001a,b) as well as of rock analogues (Herwegh et al., 1997). They were all related to the relaxation of strain compatibility in the aggregates by dynamic recrystallisation or grain boundary sliding, i.e. to strain accommodation by an additional process coming into play. At high strain, steady-state textures established, which are symmetrically disposed with respect to the shear plane.

The CPO in the grey mylonites qualitatively resembles that of Solnhofen limestone (fig. 5 in Casey et al., 1998) deformed to moderate shear strains ($\gamma = 3$ to 7). Both have monoclinic symmetry and are dominated by *c*-axis maxima 1 and 3. The texture maxima of our mylonites are more diffuse, merged together and therefore less pronounced than those from the experiments. The texture of the white mylonites corresponds rather to that of Solnhofen after large shear strain ($\gamma \geq 10$). Consequently, the asymmetric textures of the grey mylonites may reflect a transitional stage at lower finite strains, while the white mylonites represent a steady state texture characteristic for high shear strains.

This explanation is unrealistic especially in the case of the Doldenhorn nappe considering the high total shear strains from the thrust movement. As about 10 km of displacement were accommodated within a relatively narrow zone, this would have required a big competence contrast between the two mylonite types. Furthermore, a layer parallel geometry of white and grey mylonites is observed instead of fracturing or boudinage of the grey mylonites as the stronger material, thus indicating a rather moderate viscosity contrast. These arguments imply that the grey mylonites must have accommodated a shear strain comparable with that in the white ones, and that a transitional texture in the grey mylonites alone is not an acceptable interpretation.

5.4.2. Strain partitioning

Based on symmetry considerations and supported by numerical simulations (Wenk et al., 1987), Ratschbacher et al. (1991) related the texture types in calcite mylonites to the deformation regime. Textures with oblique *c*-axis

Table 3
Overview of characteristic microstructural features of grey and white calcite mylonites

	Grey mylonites	White mylonites
Grain size average	Small	Small
Grain size range	Wider	Narrow
Grain shape	More elongated	Less elongated
SPO	None or parallel to the shear plane	Oblique to the shear plane
CPO	Oblique to the shear plane	Symmetric to the shear plane
Dynamically recrystallised grains	More twinning	Less twinning
Nano-scale structured kerogen	More	Less
Rate of recrystallisation	Slower	Faster
Interpretation	Deformation microfabrics	Recrystallisation microfabrics

maxima were attributed to dominantly non-coaxial deformation (simple shear) and those with *c*-axes normal to the shear plane to primarily coaxial conditions (pure shear). Accordingly, the textures in the grey mylonites reflect non-coaxial deformation, and those in the white mylonites should have resulted from coaxial kinematics. This would have required a strain partitioning where the rotational part of the deformation is mostly accommodated by the grey mylonites.

In coaxial deformation, any microstructural component must show orthorhombic symmetry, given the protolith was isotropic (Paterson and Weiss, 1961). As the white mylonites have an SPO in oblique orientation relative to the shear plane, i.e. with monoclinic symmetry, they cannot have formed exclusively under coaxial conditions. On the other hand, the orthorhombic CPO in the white mylonites does not necessarily have to be the result of coaxial deformation. It is highly compatible with symmetry arguments and, as demonstrated in the high strain shear experiments mentioned above, simple shear may actually produce recrystallisation textures with orthorhombic symmetry. Therefore the proposed interpretation of strain partitioning between both mylonite types is abandoned here.

5.4.3. Recrystallisation rate

The third and preferred explanation can be seen again in the light of a different recrystallisation behavior between white and grey calcite mylonites (Table 3). A natural microfabric basically reflects a frozen stage of a rather dynamic system in which all crystals continuously undergo rotations (Wenk et al., 1989) and with recrystallisation, they will ultimately be replaced by new grains. The rates of lattice rotation vary as a function of the ability of the grains to accommodate shear by intracrystalline slip, which depends primarily on the crystallographic orientation. The rotation rate is especially low in so-called 'easy glide' orientations where grains are able to accommodate a considerable amount of shear strain by intracrystalline slip on a single slip systems (Schmid, 1982). Grains that rotate away from these favoured orientations quickly become harder to deform and get consumed through migration recrystallisation by grains in softer orientations (Herwegh et al., 1997). The physical reason for this behaviour is an increased defect density (dislocations, subgrains and twins) in grains with unfavoured orientations, which enhances the driving force for grain boundary migration. As discussed above, nano-scale second-phase particles induce dragging/pinning forces, which reduce the grain boundary mobility. Thus, the velocity of grain boundary migration and therefore the recrystallisation rate were somewhat smaller in grey than in white mylonites. Individual grains persisted longer in the microstructure before they became consumed again through grain boundary migration. In other words, the microstructure of the white mylonites is formed by rapid dynamic recrystallisation accompanying deformation, which results in a continuous resetting of the microfabrics. This resetting occurred similarly but slower in the grey mylonites, which therefore reflect more of a deformation microstructure. In the same way, the white mylonites possess 'recrystallisation textures' while the grey ones are more characteristic for 'deformation textures', more strongly pronouncing the texture components due to intracrystalline deformation. In addition, the Doldenhorn samples show more elongate grain shapes and flattened SPO in the grey than in the white mylonite, which has more equant grain shapes and a steeper oblique SPO. This indicates that higher incremental shear strains accommodated in individual grains of grey, rather than white, mylonites.

5.5. Doldenhorn versus Gellihorn samples

As manifest by the well-developed CPO and some SPO, all samples must have experienced a considerable amount of intracrystalline deformation during the major episodes of thrusting. This could have been interpreted as steady state flow by dislocation creep under a power law rheology, if the small grain sizes had been neglected.

An extrapolation of calcite flow laws derived from experiments (Rutter, 1974; Schmid et al., 1977, 1980; Walker et al., 1990) predicts, however, that there is no domain of power law flow for the estimated deformation conditions (Doldenhorn: $T = 613$ K, $d = 7.5$ μm; Gellihorn: $T = 543$ K, $d = 2.5$ μm). Both rocks should deform under an exponential flow law at fast strain rates (above about $10^{-10}\,s^{-1}$) requiring high differential stress of several hundred MPa. At slower strain rates, grain size sensitive

flow (stress exponent $n = 1.7$) becomes more favourable and the flow stress rapidly reduces with decreasing strain rate (e.g. at 10^{-12} s^{-1} to about 10 and 40 MPa, respectively). The ratio between the calculated stresses for Doldenhorn and Gellihorn conditions varies between 0.2 and 0.3 depending on the flow law applied and does not change with strain rate. Thus, assuming the same (unknown) strain rate for both nappes, the Doldenhorn mylonite required about one quarter of the flow stress of the Gellihorn mylonite. Applying calcite paleopiezometry (Schmid et al., 1980), this should cause a dynamically recrystallised grain size by about the same factor larger in the Doldenhorn mylonite, which is actually well the case for the samples investigated. Keeping in mind the uncertainties of such an extrapolation based on experimental flow laws, the consistency between predicted and observed grain size ratios at least supports an interpretation of grain size sensitive flow in these mylonites.

Power law (dislocation) creep becomes more favourable with increasing temperature, and starting at about 400 °C it assumes an enlarging domain separating exponential from grain size sensitive flow. Though it is not the rate limiting mechanism under either condition, the (minor) contribution of dislocation creep might therefore be even smaller for the Gellihorn than for the Doldenhorn mylonites. This would correspond to the weaker texture observed in the grey mylonite from the Gellihorn nappe compared with the grey Doldenhorn sample.

5.6. Mechanisms of grain size sensitive flow

A bulk sample usually deforms by a combination of several simultaneously active mechanisms (e.g. Pfiffner, 1982; Burkhard, 1990; Van der Pluijm, 1991; Busch and Van Der Pluijm, 1995). In particular, diffusion creep and grain boundary sliding are two mechanisms that both correspond to grain size sensitive flow laws (Poirier, 1985). Based on microstructural observations, the two mechanisms are hard to distinguish. Diffusion creep is usually inferred as a high temperature process, and may not be activated under the low peak temperatures estimated, even at geological time scales. Granular flow accommodated by material transfer via intergranular fluid (Paterson, 1995) might be a more likely process (see also McClay, 1977; Busch and Van Der Pluijm, 1995). This suggestion is supported by the observation of small grain sizes in combination with the presence of fluids (veins). Grain boundary sliding is certainly enhanced by fluids and also by impurities lubricating the grain boundaries like the nano-scale kerogens discussed above. It may well be accommodated by some intracrystalline deformation as argued for experiments of Solnhofen limestone (Casey et al., 1998).

Fluid enhanced granular flow has also been discussed for deformation of sheet silicate bearing calcite mylonites (Herwegh and Jenni, 2001). Such mica-rich calcite mylonites were reported as fine-grained rocks with a pronounced foliation, strong SPO and seismic anisotropy, but with a nearly random CPO (Burlini and Kunze, 2000). Compared to those rocks with mica content of 5 vol% and more, the investigated mylonites of the Doldenhorn and Gellihorn nappe are much purer. Hence the supply of fluids was more restricted, and intracrystalline deformation accompanied the fluid-based material transfer as an accommodating process.

6. Conclusions

Nano-scale second-phase particles influence microstructure and texture in fine-grained calcite aggregates of grey mylonites by pinning/dragging the migrating grain boundaries during deformation and dynamic recrystallisation. In the past, similar microfabrics with straight grain boundaries and without bulges and lobes were interpreted to be diagnostic for the absence of grain boundary migration recrystallisation, although in coarser grained rocks. We cannot completely rule out any post-deformational annealing that could have straightened the boundaries afterwards. However, as the fabrics still show small grain sizes, elongate grain shapes and clear CPO, there was surely no post-deformational event of static recrystallisation. The comparison of grey and white mylonites that deformed at the same lower metamorphic conditions demonstrated that grain boundary migration recrystallisation is a syn-deformational process to continuously refresh the microfabric, which depends sensitively on the content of nano-scale particles in rocks of otherwise equal composition.

In the presence of fluids, the behaviour of nano-scale organic matter is a further important feature. While highly ordered kerogens are immobile, weakly structured kerogens can apparently be transported by fluids and precipitated at new sites (e.g. in calcite veins). Thus in monotone calcite rock types, they might be used as tracers to indicate the presence of fluids during deformation as well as to detect the fluid pathways under low temperature metamorphic conditions. A question that should be addressed in future work is the behaviour of the kerogens under high temperature deformation conditions.

Finally, the interpretation of CPO obliquity needs to be clarified. An oblique CPO must always be the result of a non-coaxial deformation. Vice versa, non-coaxial deformation may produce either symmetric or oblique textures. Consequently, if a symmetric texture is observed no distinction can be made about coaxial or non-coaxial deformation, and an interpretation requires additional information, e.g. from the SPO. The differences in the CPO of white and grey mylonites have important consequences for field geologists. The oblique deformation texture in grey mylonites continues to serve as a reliable shear sense indicator while the symmetric recrystallisation texture in the white ones does not indicate any sense of movement.

Acknowledgements

We would like to thank Karl Ramseyer, Adrian Pfiffner, Martin Burkhard, Luigi Burlini and Stefan Schmid for stimulating discussions. Mr Hürlimann, F. Giacomini and Mrs Marbacher helped to operate the Leco combustion apparatus, Anne-Chantal Risold prepared TEM samples by ion-etching. We are indebted to Marcel Düggelin (SEM facility, University of Basel) for acquisition of the FEG images. Martin Casey kindly gave access to the pole figure contouring program PLOBIN. Janos Urai and an anonymous reviewer are thanked for very detailed and constructive reviews.

References

Bestmann, M., Kunze, K., Matthews, A., 2000. Evolution of a calcite marble shear zone complex on Thassos Island, Greece: microstructural and textural fabrics and their kinematic significance. Journal of Structural Geology 22, 1789–1807.

Burkhard, M., 1988. L'Helvetique de la bordure occidentale du massif de l'Aar (évolution tectonique et métamorphique). Eclogae geolgica Helvetiae 81, 63–114.

Burkhard, M., 1990. Ductile deformation mechanisms in micritic limestones naturally deformed at low temperatures (150–350 °C). In: Knipe, R.J., Rutter, E.H. (Eds.), Deformation Mechanisms, Rheology and Tectonics. Geological Society Special Publication 54, pp. 241–257.

Burkhard, M., 1993. Calcite twins, their geometry, appearence and significance as stress-strain markers and indicators of tectonic regime: a review. Journal of Structural Geology 15, 351–369.

Burlini, L., Kunze, K., 2000. Fabric and seismic properties of a Carrara marble mylonite. Physics and Chemistry of the Earth 25, 133–139.

Busch, J.P., Van Der Pluijm, B.A., 1995. Calcite textures, microstructures and rheological properties of marble mylonites in the Bancroft shear zone, Ontario, Canada. Journal of Structural Geology 17, 677–688.

Casey, M., Kunze, K., Olgaard, D.L., 1998. Texture of Solnhofen limestone deformed to high strains in torsion. Journal of Structural Geology 20, 255–267.

Cizek, Z., Borek, P., Fiala, J., Bodgain, B., 1990. New analytical method for determination and speciation of forms of carbon. Microchimica Acta 111, 163–170.

De Bresser, J.H.P., Ter Heege, J.H., Spiers, C.J., 2001. Grain size reduction by dynamic recrystallization: can it result in major rheological weakening? International Journal of Earth Sciences (Geol. Rundschau) 90, 28–45.

Doherty, R.D., Hughes, D.A., Humphreys, F.J., Jonas, J.J., Juul Jensen, D., Kassner, M.E., King, W.E., McNelley, T.R., McQueen, H.J., Rollett, A.D., 1997. Current issues in recrystallization: a review. Materials Science and Engineering A238, 219–274.

Drury, M.R., Urai, J.L., 1990. Deformation-related recrystallization processes. Tectonophysics 172, 235–253.

Evans, B., Renner, J., Hirth, G., 2001. A few remarks on the kinetics of static grain growth in rocks. International Journal of Earth Sciences 90, 88–103.

Frey, M., Teichmüller, M., Teichmüller, R., Mullis, J., Künzi, B., Breitschmid, A., Gruner, U., Schwizer, B., 1980. Very low-grade metamoprhism in external parts of the Central Alps: illite crystallinity, coal rank and fluid inclusion data. Eclogae geolgica Helvetiae 73, 173–203.

Herwegh, M., 2000. A new technique to automatically quantify microstructures of fine grained carbonate mylonites: two-step etching combined with SEM imaging and image analysis. Journal of Structural Geology 22, 391–400.

Herwegh, M., Jenni, A., 2001. Granular flow in polymineralic rocks bearing sheet silicates: new evidence from natural examples. Tectonophysics 332, 309–320.

Herwegh, M., Handy, M.R., Heilbronner, R., 1997. Temperature and strain rate dependent microfabric evolution in monomineralic mylonite: evidence from in situ deformation of a rock analogue. Tectonophysics 280, 83–106.

Hirth, G., Tullis, J., 1992. Dislocation creep regimes in quartz aggregates. Journal of Structural Geology 14, 145–159.

Hornbogen, K., Köster, U., 1978. Recrystallization of two-phase alloys. In: Haessner, F. (Ed.). Recrystallization of Metallic Materials. Dr Riederer Verlag, Stuttgart, pp. 159–194.

Humphreys, F.J., Hatherly, M., 1996. Recrystallization and Related Annealing Phenomena. Pergamon Press, Oxford, 497pp.

Knipe, R.J., 1989. Deformation mechanisms—recognition from natural tectonites. Journal of Structural Geology 11, 127–146.

Kocks, U.F., Tome, C.N., Wenk, H.-R., 1999. Texture and Anisotropy. University Press, Cambridge 676pp.

McClay, K.R., 1977. Pressure solution and coble creep in rocks and minerals, a review. Journal of the Geological Society London 134, 57–70.

Means, W.D., 1981. The concept of steady-state foliation. Tectonophysics 78, 179–199.

Olgaard, D.L., 1990. The role of second phase in localizing deformation. In: Knipe, R.J., Rutter, E.H. (Eds.), Deformation Mechanisms, Rheology and Tectonics. Geological Society Special Publication 54, 175–181.

Olgaard, D.L., Evans, B.E., 1986. Effect of second-phase particles on grain growth in calcite. Journal of the American Ceramic Society 69, C272–C277.

Olgaard, D.L., Evans, B.E., 1988. Grain growth in synthetic marbles with added mica water. Contributions to Mineralogy and Petrology 100, 246–260.

Panozzo, R., 1983. Two-dimensional analysis of shape-fabric using projections of digitized lines in a plane. Tectonophysics 95, 249–279.

Paterson, M.S., 1995. A theory for granular flow accommodated by material transfer via intergranular fluid. Tectonophysics 245, 135–151.

Paterson, M.S., Weiss, L.E., 1961. Symmetry concepts in the structural analysis of rocks. Geological Society of America Bulletin 72, 841–882.

Pieri, M., Kunze, K., Burlini, L., Stretton, I., Olgaard, D.L., Burg, J.P., Wenk, H.R., 2001a. Texture development in calcite through deformation and dynamic recrystallization at 1000 K during torsion of marble to large strains. Tectonophysics 330, 119–140.

Pieri, M., Burlini, L., Kunze, K., Stretton, I., Olgaard, L., 2001b. Rheological and microstructural evolution of Carrara marble with high shear strain: results from high temperature torsion experiments. Journal of Structural Geology 23, 1393–1413.

Pfiffner, O.A., 1982. Deformation mechanisms and flow regimes in limestones from the Helvetic zone of the Swiss Alps. Journal of Structural Geology 4, 429–442.

Pfiffner, O.A., Sahli, S., Stäuble, M., 1997. Compression and uplift of the external massifs in the Helvetic zone. In: Pfiffner, O.A., Lehner, P., Heitzmann, P., Mueller, St., Steck, A. (Eds.). Results of NRP 20. Birkhäuser, pp. 139–153.

Poirier, J.P., 1985. Creep of Crystals—High-temperature Deformation Processes in Metals, Ceramics and Minerals. Cambridge University Press, Cambridge.

Ratschbacher, L., Wenk, H.-R., Sintubin, M., 1991. Calcite textures: examples from nappes with strain-path partitioning. Journal of Structural Geology 13, 369–384.

Rutter, E.H., 1974. The influence of temperature, strain rate and interstitial water in the experimental deformation of calcite rocks. Tectonophysics 22, 311–334.

Rutter, E.H., Casey, M., Burlini, L., 1994. Preferred crystalplastic orientation development during the plastic and superplastic flow of calcite rocks. Journal of Structural Geology 16, 1431–1446.

Schmid, J., 1997. The genesis of white marble: geological causes and archaeological applications. Unpublished Ph.D. thesis, University of Berne, Switzerland.

Schmid, S.M., 1976. Rheological evidence for changes in the deformation mechanism of Solnhofen limestone towards low stresses. Tectonophysics 31, T21–T28.

Schmid, S.M., 1981. Laboratory experiments on rheology and deformation mechanisms in calcite rocks and their application to studies in the field. Mitteilungen aus dem Geol. Institut, der ETH und der Univ. Zürich N.F. 241, 106pp.

Schmid, S.M., 1982. Microfabric studies as indcators of deformation mechanisms and flow laws operative in mountain building. In: Hsü, K.J. (Ed.). Mountain Building Processes. Academic Press, London, pp. 95–110.

Schmid, S.M., Paterson, M.S., Boland, J.N., 1977. Superplastic flow in fine-grained limestone. Tectonophysics 43, 257–291.

Schmid, S.M., Paterson, M.S., Boland, J.N., 1980. High temperature flow and dynamic recrystallization in Carrara Marble. Tectonophysics 65, 245–280.

Schmid, S.M., Casey, M., Starkey, J., 1981. The microfabric of calcite tectonites from the Helvetic nappes (Swiss Alps). In: McClay, K., Price, N.J. (Eds.), Thrust and Nappe Tectonics. Geological Society Special Publication 9, pp. 151–158.

Schmid, S.M., Panozzo, R., Bauer, S., 1987. Simple shear experiments on calcite rocks: rheology and microfabric. Journal of Structural Geology 9, 747–778.

Urai, J.L., Means, W.D., Lister, G.S., 1986. Dynamic recrystallization of minerals. In: Hobbs B.E., Heard H.C. (Eds.), Mineral and Rock Deformation: Laboratory Studies—The Paterson Volume. Geophysical Monographs 36, pp. 161–199.

Van Der Pluijm, B.A., 1991. Marble mylonites in the Bancroft shear zone, Ontario, Canada: microstructures and deformation mechanisms. Journal of Structural Geology 13, 1125–1135.

Walker, A.N., Rutter, E.H., Brodie, K.H., 1990. Experimental study of grain-size sensitive flow of synthetic, hot pressed calcite rocks. In: Knipe, R.J., Rutter, E.H. (Eds.), Deformation Mechanisms, Rheology and Tectonics. Geological Society Special Publication 54, pp. 259–284.

Wenk, H.-R., Takeshita, T., Bechler, E., Erskine, B.G., Matthies, S., 1987. Pure shear and simple shear calcite textures. Comparison of experimental theoretical and natural data. Journal of Structural Geology 9, 731–745.

Wenk, H.-R., Canova, G., Molinari, A., Kocks, U.F., 1989. Viscoplastic modelling of texture development in quartzite. Journal of Geophysical Research 94B, 17895–17906.